Raman spectroscopy of biosignatures in methane-related microbialites

Tim Leefmann[1,2] *; Martin Blumenberg[3]; Burkhard C. Schmidt[4] & Volker Thiel[2] *

[1]*Department of Earth and Planetary Sciences, Macquarie University, Sydney, NSW 2109, Australia; Email: tim.leefmann@mq.edu.au*
[2]*Department of Geobiology, Geoscience Centre, Georg-August University Göttingen, Goldschmidtstr. 3, 37077 Göttingen, Germany; Email: Volker.Thiel@geo.uni-goettingen.de*
[3]*Federal Institute for Geosciences and Natural Resources (BGR), Stilleweg 2, 30655 Hannover, Germany; Email: Martin.Blumenberg@bgr.de*
[4]*Department of Experimental and Applied Mineralogy, Geoscience Centre, Georg-August University Göttingen, Goldschmidtstr. 1, 37077 Göttingen, Germany*

* corresponding authors

Göttingen Contributions to Geosciences
www.gzg.uni-goettingen.de

77: 113-122, 7 figs. 2014

A major challenge in geobiological studies is the localization of organic compounds in a mineral matrix. Raman spectroscopy is here potentially powerful as it can be employed directly on rock surfaces and is capable of the characterization of organic and inorganic compounds in one analyzing step. In this study we tested Raman spectroscopy to approach the organic matter information locked in the complex mineral phase association of methane-related carbonate chemoherms of different age (Hydrate Ridge, Lincoln Creek, Münder Formation, Black Sea). Our data show that Raman spectroscopy allows detecting differences in the amount of organic material in geobiological samples on a micrometer scale. Particularly for the microbialites from Hydrate Ridge and the Lincoln Creek Formation, these studies were able to distinguish on a mm-scale fossilized biofilms of methanotrophic consortia from precipitates that were not directly mediated by microorganisms. However, Raman spectroscopy did not allow for a compound-class specific characterization of the organic material within the microbialite samples. A laser excitation wavelength of 244 nm was determined as most promising for the analysis of organic matter contents of carbonates, as it largely avoids autofluorescence. Comparisons with published extract-based studies (GC-MS) of the same samples demonstrate that the different techniques cannot replace each other, but should rather be used in conjunction in geobiological studies.

Received: 05 July 2013
Accepted: 06 January 2014

Subject Areas: Geobiology, biogeochemistry, microbialites

Keywords: Biosignatures, Raman spectroscopy, cold seep carbonates, biomarker

Introduction

In studies of microbially controlled systems such as biofilms, stromatolites and other microbialites on small scales, the exact localization of organic compounds represents a major analytical challenge. Because of the consumption of relatively high sample amounts (typically >1000 mg), extraction-based biomarker techniques provide bulk information, and their spatial resolution usually stands isolated from the microscopic and inorganic techniques that operate at the microscopic level (e.g., SEM/EDX, EMS, LA-ICP-MS). In geobiological studies this problem makes it difficult to associate distinctive mineral precipitates with the former presence of particular microbes and by implication, biogeochemical pathways. Likewise it is difficult to estimate as to what extent organic substances retain their once existing spatial association with an inorganic mineral phase during diagenesis. Ap-

proaching higher spatial resolution in the analysis of organic biomarkers in inhomogeneous samples is therefore a highly desirable goal and several recent biomarker studies aimed in that direction. These studies encompassed, for instance, the phase specific fatty acid analysis of fossil carbonate concretions using conventional gas chromatography-mass spectrometry (Pearson et al. 2005; Leefmann et al. 2008; Hagemann et al. 2013), microanalysis of organic fossils using laser pyrolysis-GC-MS (La-Py-GC-MS; Greenwood et al. 1998), and mapping of organic compounds using Time-of-Flight Secondary Ion Mass Spectrometry (ToF-SIMS, Toporski et al. 2002; Thiel et al. 2007).

Here we employed Raman spectroscopy to approach the organic matter information locked in complex mineral phase association of methane-related carbonate chemoherms. Methane–derived carbonate formation is particularly pronounced at cold seeps, areas on the ocean floor where methane-rich fluids or gas escapes from the sediment into the water column. It is commonly accepted that carbonate precipitation is due to the microbial anaerobic oxidation of upward migrating methane by downward migrating sulfate coming from the sea water (AOM; Iversen & Jörgensen 1985; Reeburgh 1976; Barnes & Goldberg 1976). The exact mechanisms of AOM have not been finally clarified, but probably involve the oxidation of methane (CH_4) to carbon dioxide (CO_2) by methanotrophic archaea via reverse methanogenesis (Gal'chenko 2004) and sulfate-reduction to hydrogen sulphide (HS^-) by sulfate reducing bacteria (SRB) according to the sum reaction

$$CH_4 + SO_4^{2-} \rightarrow HCO_3^- + HS^- + H_2O$$

(Valentine & Reeburgh 2000)

Since the mid 1980s active cold seeps have been discovered at various ocean margin settings (Suess et al. 1985; Polikarpov et al. 1992; Greinert et al. 2002; Werne et al. 2004). Beside the recent cold seeps, fossil counterparts of Cenozoic, Mesozoic and even Palaeozoic age have been found (Campbell et al. 2002; Peckmann & Thiel 2004; Birgel et al. 2008). At recent cold seep sites diverse types of carbonates occur (Greinert et al. 2001), but the most common chemoherm carbonates are aragonites and low Mg-calcites (Peckmann et al. 2001; Reitner et al. 2005; Teichert et al. 2005). Whether aragonite or low Mg-calcite is precipitated, is not yet understood but assumed to depend on sulfate and phosphate concentrations, carbonate supersaturation and the viscosity of the growth medium (Peckmann et al. 2001).

Our study aimed to test the utility of Raman spectroscopy for directly probing the distribution of organic matter in a number of methane-related carbonates, and to establish a linkage between the past activity of microorganisms and the precipitation of distinctive mineral phases at cold seeps. Modern micro-Raman systems comprise one or more lasers which are focused through a microscope on the sample. Such micro-Raman systems are capable of analyzing the organic and inorganic features of samples with lateral resolutions at the micrometer scale. Moreover, by the introduction of confocal microscopy the spatial resolution along the optical axis has been additionally improved. However, the occurrence of high intensity fluorescence is the major problem in Raman spectroscopy, especially when applying this technique to biological samples containing fluorophores. As the Raman signal is usually comparatively low in intensity, the occurrence of fluorescence complicates the identification of individual Raman-active vibrational modes by masking the corresponding Raman bands. However, recent advances in technology have addressed this problem. Fluorescence effects may be decreased or avoided by using the Resonance Raman Effect (RRE; e.g., Kiefer 1995), Surface-Enhanced Raman Scattering (SERS; e.g., Kneipp et al. 1999), or deep ultra violet (UV) Raman spectroscopy (e.g., Frosch et al. 2007; Tarcea et al. 2007).

In this study we used deep UV-Raman spectroscopy, which allows to completely avoid interference of Raman and fluorescence signals, because the latter do not occur at excitation wavelengths below 250 nm. Furthermore, as many inorganic and organic materials have absorption bands in the deep UV-region, a laser excitation wavelength <250 nm will likely result in the resonance enhancement of certain Raman bands (e.g., Tarcea et al. 2007).

Using the deep UV-laser the small-scale distribution of organic matter within different mineral phases of methane-derived microbialites was analyzed for (1) Hydrate Ridge (Pleistocene, off Oregon, USA), (2) Lincoln Creek Formation (Oligocene, Washington State, USA), (3) Münder Formation (Late Jurassic, NW-Germany), and (4) modern methane seep associated microbial mats from the Black Sea. Published data obtained by our group from similar samples using coupled gas chromatography-mass spectrometry (GC-MS), were used as a reference and for comparing the analytical capabilities of both techniques (Leefmann et al. 2008; Hagemann et al. 2013).

Material and methods

Samples

– Hydrate Ridge, SE-Knoll chemoherm, NW-Pacific Ocean –

Hydrate Ridge is located 90 km offshore central Oregon, USA. The ridge, extending 25 km in N–S and 15 km in E–W direction, is morphologically divided into a northern and a southern summit. The up to 90 m high SE-Knoll chemoherm is located about 15 km SE from the southern summit of Hydrate Ridge. The samples were taken from a carbonate block collected during cruise SO165/2 of research vessel 'Sonne' in August 2002. The block was gathered directly from the top of the SE-Knoll chemoherm using a television grab (TVG; Station 230-1, TVG-13, 44:27.0440°N, 125:01.8000°W, 615 m water depth).

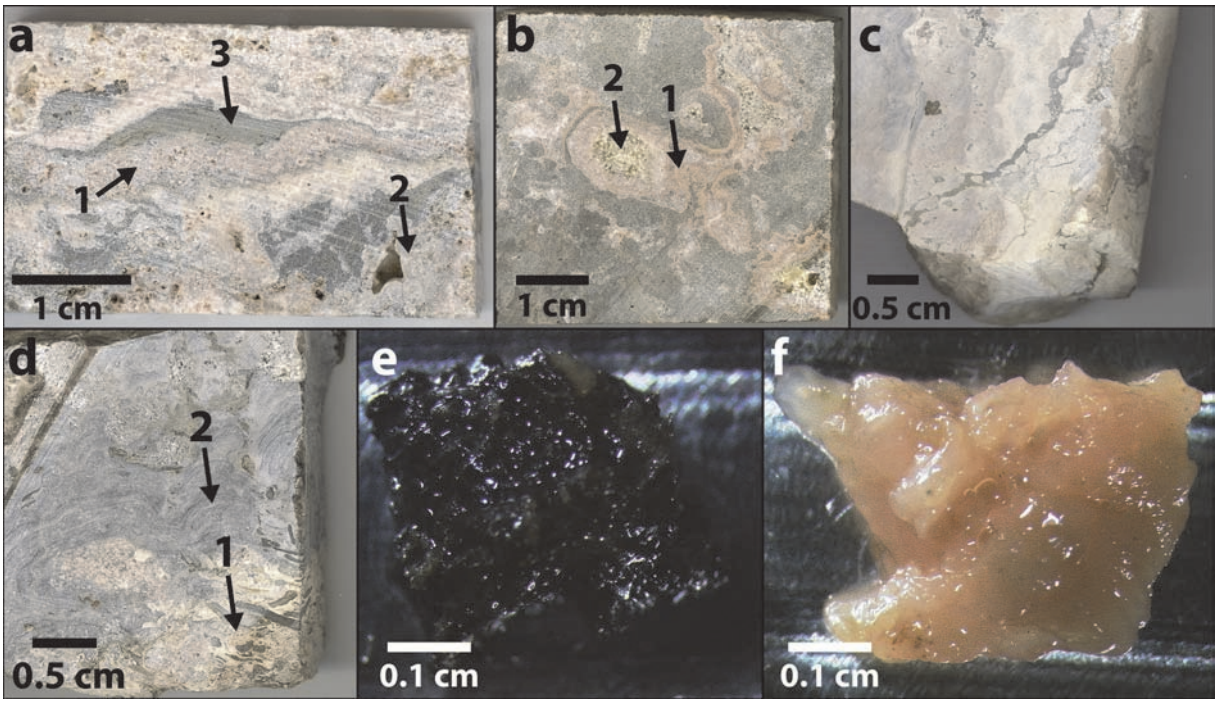

Fig. 1: Mineral phases and microbial mat types analyzed by Raman spectroscopy. (**a**) Hydrate Ridge sample with arrows marking (1) whitish aragonite, (2) lucent aragonite, and (3) gray micrite; (**b**) Lincoln Creek Formation sample with arrows marking (1) yellow aragonite, and (2) equant calcite spar; (**c**) initial clast of Münder Formation sample; (**d**) Münder Formation sample with arrows marking (1) growth phase 1, and (2) growth phase 2; (**e**) black microbial mat type of Black Sea samples; (**f**) pink microbial mat type of Black Sea samples.

From this block a core of 50 mm in diameter was drilled, which was later cut lengthwise resulting in two transverse sections. From one of these sections, the analyzed samples were taken.

The drill core section contains three closely interfingered, major carbonate types. These carbonate types (first described by Teichert et al. 2005) consist of a macroscopically opaque, cryptocrystalline variety of aragonite ranging in color from white to pinkish and brownish (*whitish aragonite*), a translucent, botryoidal aragonite consisting of fibrous, acicular crystals (*lucent aragonite*), and a gray, microcrystalline carbonate with varying content of Mg-calcite and various components, namely shell fragments, pellets containing pyrite, peloids and detrital quartz, and feldspar grains (*gray micrite*; Fig. 1a)

– Lincoln Creek Formation, USA –

Within the Oligocene Lincoln Creek Formation, which is exposed within river valleys of the south-eastern Olympic Peninsula, Washington, USA, several cold seep carbonate deposits have been observed (Peckmann et al. 2002). Samples of these cold seep carbonates were retrieved through an expedition to the Olympic Peninsula in September 2004. Within the cold seep carbonates several different phases, namely *gray micrite*, *yellow aragonite*, *clear aragonite*, and *equant calcite spar* were distinguished and analyzed for their biomarker content by GC-MS (Fig. 1b; Hagemann et al. 2013).

– Münder Formation, Germany –

A stromatolite sample was retrieved from a limestone quarry near the village of Thüste, located 30 to 50 km southeast of Hannover, Germany. The sample site is located in the centre of the Hils Syncline, a halotectonic depression that formed during the late Late Jurassic (Thitonian) to the lowermost Cretaceous (Berriasian). Within the quarries, oolithic limestones are overlain by a dark, well-stratified to laminated marlstone bed with prominent occurrences of stromatolites. The analyzed stromatolite sample was comprised of three distinct phases, namely the *initial clast*, and the *growth phases 1* and *2* (Figs. 1c, d; for a detailed description, see Arp et al. 2008). *Growth phase 1* shows irregular dendroid stromatolite columns and is composed of hemispheres with a vesicular, spar-cemented core veneered by brownish to dark gray microcrystalline laminae. In contrast *growth phase 2* is characterized by regular columns. This dark gray to gray phase includes stromatolithic lamination as a result of alternation of porous, clotted laminae with elongated, angular crystal traces. The microfabric of the *initial clast* is identical to the fabric of the *growth phases 1* and *2*, but discontinuities of growth are more abundant (for a detailed petrographic description see Arp et al. 2008).

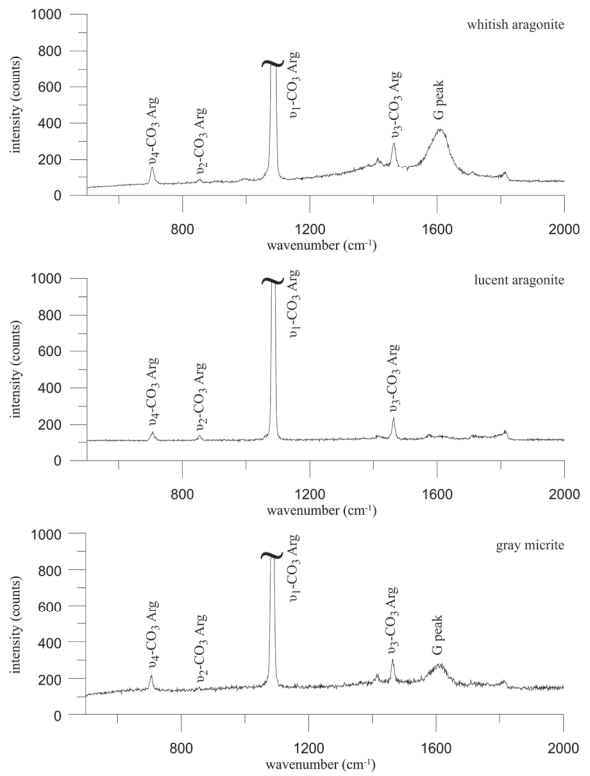

Fig. 2: UV-Raman spectra of distinct phases of samples from Hydrate Ridge, SE-Knoll chemoherm. (Arg = aragonite; peak assignments are discussed in text).

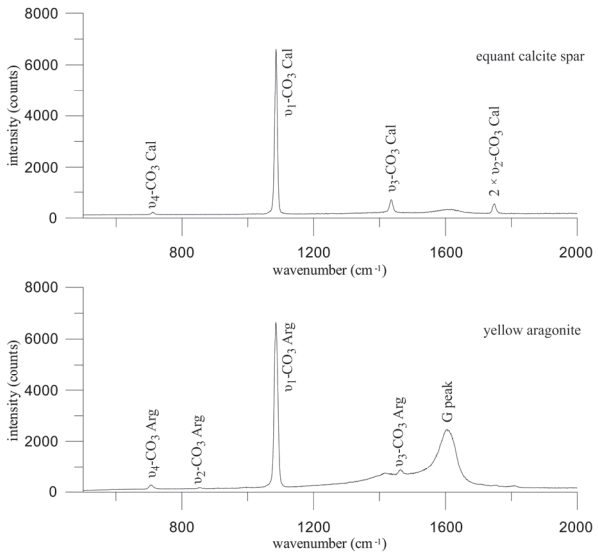

Fig. 3: UV-Raman spectra of distinct phases of samples from the Lincoln Creek Formation. (Cal = calcite; Arg = aragonite; peak assignments are discussed in text).

– Black Sea –

Several studies have reported the occurrence of methane seepage in the NW' Black Sea (e.g., Egorov et al. 1998). The combination of methane seepage and anoxic bottom water conditions results in the shifting of the AOM-activity from the sediments into the water column. As a consequence carbonate towers up to 4 m in height grow into the anoxic water column (Pimenov et al. 1997; Michaelis et al. 2002; Reitner et al. 2005). Microbial mats mediating AOM were found to be associated with these carbonate build-ups. Samples were obtained from cruise 317-2 of research vessel 'Poseidon' to the lower Crimean shelf of the NW' Black Sea in September 2004. By using the manned submersible 'Jago', samples of microbial mats associated with carbonate towers were taken at water depths of 203 m (Station No.752; 44°46.41' N, 31°58.84' E), 235 m (Station No.744; 44°46.47' N, 31°59.52' E), 229 m (Station No.716; 44°46.49'N, 31°59.55'E), and 221 m (Station No.744; 44°46.48'N, 31°59.49'E), respectively. The samples were immediately frozen on board of RV Poseidon and stored at -20°C. Two different mat types were macroscopically distinguished, namely a *black* and a *pink mat* type (Figs. 1e, f). From each mat type, one sample was analyzed by means of Raman spectroscopy

Sample preparation

To avoid contamination of the sample surface by organic compounds, all preparation tools with direct sample contact (blade saw, spatula, pipettes, and object slides) were carefully pre-cleaned using acetone.

Using a rock saw 3 x 5 cm sized slabs were cut out of the original samples from Hydrate Ridge, Lincoln Creek, and Münder Formation. After preparation, the rock samples were stored enveloped in aluminium foil until measurement. Small pieces of the mat samples from the Black Sea were transferred on an object slide using a spatula, and immediately measured with the Raman spectrometer.

Raman spectroscopy

The micro-Raman system (Horiba Jobin Yvon LabRAM 800 UV; Table 1) used is equipped with a 244 nm UV-laser, which was operated at 25 mW at the laser exit. Depending on the sample the initial laser power was reduced to 1 %, 10 %, 25 %, or 50 % by using different filters. The laser beam was focused on the samples by an OFR LMV-40x-UVB objective with a numerical aperture of 0.5. The confocal hole diameter was set to 200 µm. The Raman scattered light was dispersed by a 2400 l/mm grating on a liquid nitrogen cooled CCD detector with 2048 x 512 pixels, yielding a spectral dispersion of better than 1.05 cm^{-1} per pixel. Raman spectra in the range from 300–4000 cm^{-1} were obtained in 2 spectral windows. Acquisition times were 2 times 5–300 s per window. A diamond standard with a major peak at 1332.0 cm^{-1} was used for calibration of the spectrometer.

Line profile measurements on Hydrate Ridge and Lincoln Creek Formation samples were carried out using a motorized xy-stage, controlled by the HORIBA Jobin Yvon LabSpec software version 5.19.17. Peak integrals of line profile measurements were calculated from the background corrected spectra.

Table 1: Hardware specifications of the used micro-Raman system (NA = numerical aperture).

	manufacturer	model / specifications
laser	COHERENT	Innova 90C FreD Ion Laser / λ=244 nm / output power up to 100 mW
microscope	Olympus	BX41
objectives	Optics For Research	LMV-10x-UVB, NA 0.25
	Optics For Research	LMV-40x-UVB, NA 0.50
x-y-stage	Märzhauser	EK32 75x50
spectrometer	HORIBA Jobin Yvon	LabRAM HR 800 UV / focal lenght: 800 mm /gratings: 600, 1200, 2400 / filter: D03=50 %, D06=25 %, D1=10 %, D2=1 %, D3=0.1 %, D4=0.01 % of laser output power
detector	HORIBA Jobin Yvon	CCD Symphony LN2-Series / 2048 × 512 Pixel / image area: 26.6 mm × 6.9 mm

Results

The peaks detected in the cold seep samples are exclusively located in the range between 700 cm^{-1} and 1900 cm^{-1}. Peaks below 500 cm^{-1} could not be detected by UV-Raman spectroscopy due to technical limitations of the UV-notch filter systems.

– Hydrate Ridge, SE-Knoll chemoherm, NW-Pacific Ocean –

All spectra obtained from the distinct phases of the Hydrate Ridge samples showed a similar peak pattern (Fig. 2).

In the UV-Raman spectra, strong peaks occurred around 1086 cm^{-1} and 1609 cm^{-1} and medium intensity peaks around 706 cm^{-1} and 1464 cm^{-1}. Peaks of weak intensity were found around 854 cm^{-1}, 1415 cm^{-1}, 1710 cm^{-1}, and 1814 cm^{-1}. No fluorescence effects were observed when using 244 nm as excitation wavelength.

– Lincoln Creek Formation, USA –

The spectra from the *yellow aragonite* and the *equant calcite spar* were similar in peak distribution (Fig. 3). The UV-Raman spectra of both phases showed a strong band around 1083 cm^{-1}. Moreover, a band at 1606 cm^{-1} was detected, which was strongly variable in intensity. Medium intensity bands at 1435 cm^{-1} (*equant calcite spar)*, 1463 cm^{-1} (*yellow aragonite*) and 708 cm^{-1}, and weak peaks around 1749 cm^{-1} complete the spectra.

– Münder Formation, Germany –

The UV-Raman spectra obtained from the Münder formation samples showed five distinct peaks (Fig. 4). Strong peaks were detected around 1085 cm^{-1} and 1600 cm^{-1}. The latter peak is enclosed by two medium intensity peaks at 1434 cm^{-1} and 1749 cm^{-1}, respectively. A weak peak was detected at 711 cm^{-1}. Notably, in spectra from the *growth phase 1* the peak at 1600 cm^{-1} showed a higher intensity signal as the peak at 1085 cm^{-1} (Fig. 4).

– Black Sea –

The UV-Raman spectra of the microbial mat samples from the Black Sea showed a high intensity peak with a maximum around 1605 cm^{-1} and a broad shoulder towards lower Raman shifts (Fig. 5). In the pink mat type further medium intensity peaks were observed at 918 cm^{-1} and 998 cm^{-1} and 1090 cm^{-1}.

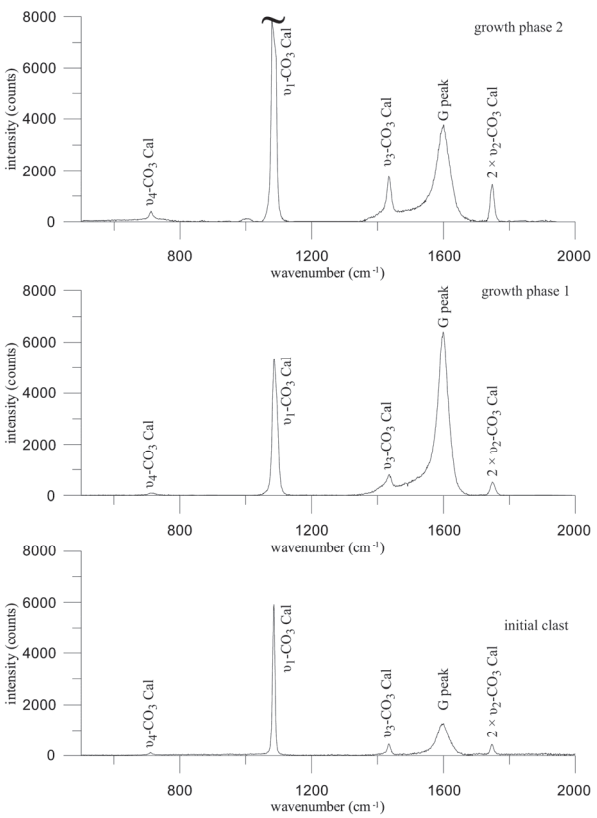

Fig. 4: UV-Raman spectra of distinct phases of samples from the Münder Formation. (Cal = calcite; peak assignments are discussed in text).

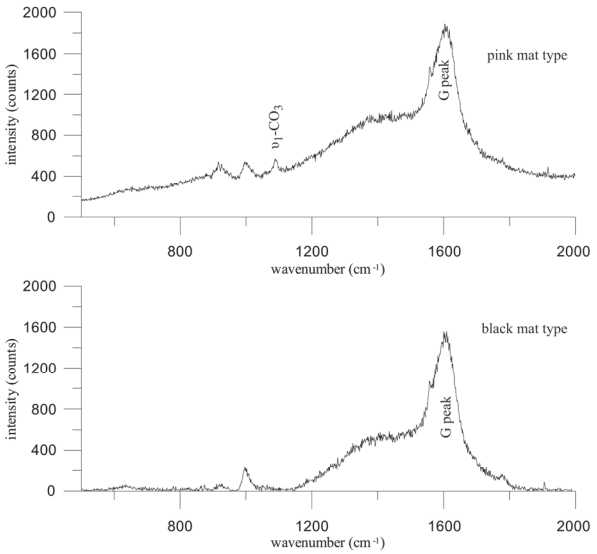

Fig. 5: UV-Raman spectra of distinct phases of microbial mat samples from the Black Sea. (peak assignments are discussed in text).

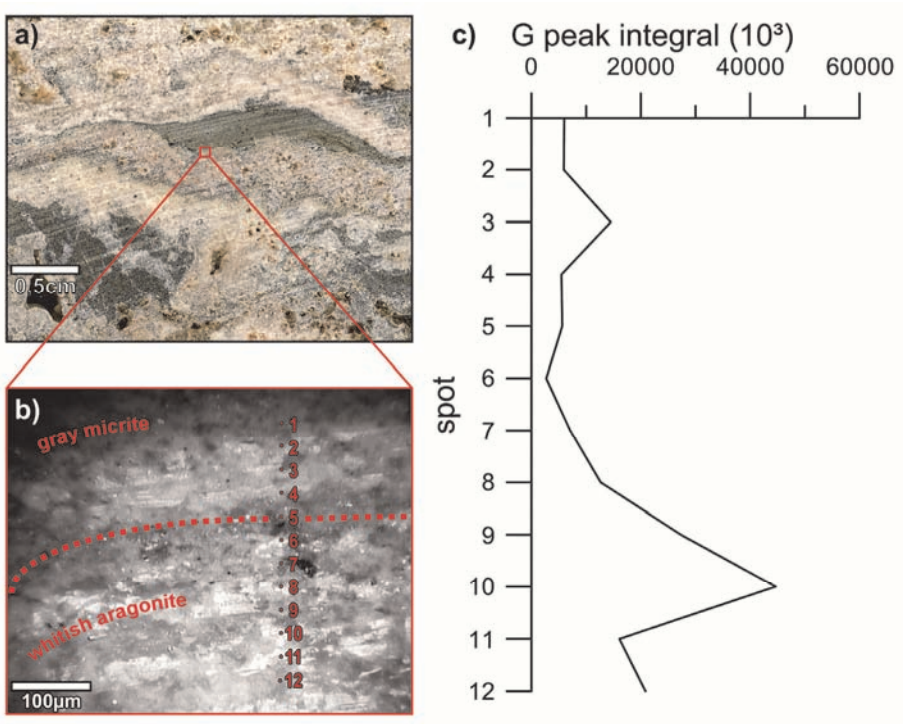

Fig. 6: Raman line profile of Hydrate Ridge microbialite using UV-laser (**a**) reflected light image of analyzed sample surface, (**b**) UV-camera image of gray micrite and whitish aragonite with marked line profile spots, (**c**) diagram of G peak integral *vs.* spot number, (G peak integral = 1548–1640 cm^{-1}).

Discussion

– Hydrate Ridge, SE-Knoll chemoherm, NW-Pacific Ocean –

Previous GC-MS studies of the analyzed Hydrate Ridge samples revealed strongly differing biomarker patterns in the three carbonate phases. This was interpreted to reflect different modes of formation (for a detailed discussion see Leefmann et al. 2008). Briefly, high amounts of AOM-specific lipid biomarkers observed in the *whitish aragonite*, such as archaeol, *sn*-2-hydroxyarchaeol, and non-isoprenoidal dialkyl glycerol diethers (DAGEs), indicate that microorganism mediating AOM were involved in the formation of this specific phase. Moreover, the abundance of *sn*-2-hydroxyarchaeol suggested that anaerobic methanotrophic archaea of the phylogenetic 'ANME-2' group played an important role among the ancient methane-consuming community (Blumenberg et al. 2004). The high amounts of DAGEs probably originated from the syntrophic SRBs of the AOM-consortia. By contrast, the *lucent aragonite* was found to be extremely lean in organic compounds, and even the lipid traces observed were probably due to contamination from other phases during sample preparation (Leefmann et al. 2008). The low biomarker concentrations reveal that this carbonate phase did not include fossilized microorganisms and suggests a mode of formation that was not directly mediated by microorganisms. The occurrence of both, AOM-specific (e.g., archaeol) and allochthonous (e.g., sterols, perylene) biomarkers in the *gray micrite* indicated, that this phase largely consists of allochthonous, i.e., sedimentary material cemented by authigenic AOM-derived carbonates (Leefmann et al. 2008).

Most Raman signals observed in the analysis of three carbonate phases can be attributed to the carbonate mineralogy (Fig. 2). The peak at 706 cm^{-1} represents the υ_4 in-plane bending mode of the carbonate-ion. The weak peak at 854 cm^{-1} can be attributed to the υ_2 mode of the carbonate ion (Frech et al. 1980). The υ_1 mode of the carbonate ion is represented by the peak at 1086 cm^{-1}. According to Frech et al. (1980), the peak at 1464 cm^{-1} arises from the υ_3 mode of the carbonate ion. Frech et al. (1980) also mention a broad feature around 1420 cm^{-1}, which may correspond to the peak at 1415 cm^{-1} observed in the UV-Raman spectra. However, the band observed in the Raman spectra at 1415 cm^{-1} is rather sharp and might thus arise from a different source. The weak peaks around 1710 cm^{-1} and 1814 cm^{-1} could not be assigned to certain vibrational modes, but they were also observed within spectra of pure aragonite (not shown). The peak observed around 1609 cm^{-1} is attributed to C-C bonds, and most likely arises from carbonaceous matter bound in the samples. For ordered, graphite-like structures this peak (referred to as G peak in the following) occurs as a sharp peak at 1575 cm^{-1}, depending on the used laser excitation wave length. Broader G peaks around 1600 cm^{-1} are common features of disordered carbonaceous materials such as kerogens. In the spectra recorded in our study, the occurrence of such broad G peaks may indicate potential alteration of the organic matter from high laser power. In spectra of disordered carbonaceous materials, the G peak is accompanied by D peaks (Pasteris & Wopenka 2003).

When using UV-excitation wavelengths, however, the D peaks greatly decrease in intensity, and were below detection limit in the spectra recorded here.

Except for the G peak no peaks specific for individual functional groups of organic compounds were observed in the spectra of the Hydrate Ridge samples. The intensity of the G peak may thus be plausibly used as a measure of organic carbon content in the mineral phases. By the line profiles, the coupling of intensity of the G peak to the individual carbonate phases should be revealed. Fig. 6 shows the integral of the broad G peak as a function of the measurement spot. The figure clearly shows that the intensity of the broad G peak decreases towards the *gray micrite*. This may be due to higher organic carbon contents in the whitish aragonite than in the *gray micrite*.

In the second profile carried out at the interfaces of *whitish* and *lucent aragonite*, the G peak integral graph shows a decrease from the *whitish* towards the *lucent aragonite* phase (Fig. 7).

Both profiles (Figs. 6, 7) clearly support the GC-MS results with respect to the biomarker content reported in Leefmann et al. (2008). Based on this experiment, it is evident that Raman spectroscopy can reveal differences in the organic carbon content of the individual mineral phases at a microscopic scale.

Summarizing, the Raman analyses of the Hydrate Ridge samples clearly indicate preferred aragonite mineralogy of all phases studied, and considerable differences in the amounts of (disordered) organic material.

– Lincoln Creek Formation, USA –

Like for the Hydrate Ridge materials, GC-MS analysis conducted on the Lincoln Creek carbonates by Hagemann et al. (2013) revealed strong differences in the distribution of lipid biomarkers between the distinct phases. The high abundance of AOM-specific biomarkers in the *yellow aragonite* was interpreted as to reflect an AOM-derived precipitate, i.e., a fossilized AOM-biofilm. Accordingly, a low abundance of lipid biomarkers in the *equant calcite spar* was assumed to represent a late diagenetic origin.

In the Raman spectra of the *yellow aragonite* and the *equant calcite spar*, most peaks represent the aragonite or calcite mineralogy, respectively (Fig. 3). The peak at 1463 cm^{-1} can be attributed to υ_3 mode of the carbonate ion in aragonite, whereas the peak at 1435 cm^{-1} is consistent with the υ_3 mode of the carbonate ion in calcite. Likewise, the peaks at 708 cm^{-1}, and 1085 cm^{-1} can be assigned to the carbonate ion. The peak at 1749 cm^{-1} can be assigned to the $2x\upsilon_2$ mode of the carbonate ion (Urmos et al. 1991). The differences in lipid biomarker content between the phases revealed by GC-MS analysis were reflected in the Raman spectra by the strong differences in the abundance of the G peak at 1606 cm^{-1}. However, no further peaks representing organic compounds were observed.

– Münder Formation, Germany –

Previous GC-MS-analyses on the same Thüste stromatolites as analyzed in this study revealed strongly ^{13}C-depleted sulfurized hydrocarbon biomarkers (Arp et al. 2008). In conjunction with other indications this was interpreted as to reflect stromatolithic carbonate $CaCO_3$ precipitation near the oxic–anoxic interface, as a result of intensive bacterial sulfur cycling and AOM, rather than of photosynthetic activity. Further GC-MS studies revealed a variety of biomarkers, but no systematic differences in the biomarker patterns between the individual growth phases were observed. However, the total amount of lipid biomarkers showed slight variations between the phases. In the Raman spectra, most peaks (711 cm^{-1}, 1085 cm^{-1}, 1434 cm^{-1} and 1749 cm^{-1}) observed in the spectra of the samples from Thüste can be assigned to calcite (Fig. 4). The only signal interpreted to originate from organic compounds is the G peak around 1600 cm^{-1}, which is markedly strong in the spectra of *growth phase 1* and thus suggests a higher organic content of this phase compared to the initial clast and *growth phase 2*. However, in the absence of Raman line profile measurements crosscutting the three phases, this interpretation must remain speculative.

– Black Sea –

Previous GC-MS analyses and compound specific isotope analyses of biomarkers from similar Black Sea mats indicated that lipids in both black and the pink variety were sourced by Archaea and SRB involved in AOM (Blumenberg et al. 2004). Furthermore, the typical compounds observed were similar to those reported from Hydrate Ridge (see above), with somewhat different distributions of phylogenetic groups in the different mat types, respectively.

In the Raman spectra of the pink mat type, the peak observed around 1090 cm^{-1} probably arises from carbonate particles within the mat (Fig. 5). The major peak at ~1605 cm^{-1} found within the UV-Raman spectra corresponds to the peak of disordered carbonaceous material found in the microbialites. However, it should be noted that the peak shape is more asymmetric than the G peaks in the spectra from the microbialite samples from the Hydrate Ridge, Lincoln Creek and the Münder Formation (Figs. 2–4). Further peaks at 918 cm^{-1} and 998 cm^{-1} might reflect vibrational modes of organic molecules, as they were not observed within the UV-Raman spectra of the carbonate samples. The spectrum of the black microbial mat showed a slightly lower signal intensity of the G peak than the pink microbial mat. In contrast to biomarker differences as been obvious from GC-MS analyses, however, no major differences were found between both mat types by Raman spectroscopy.

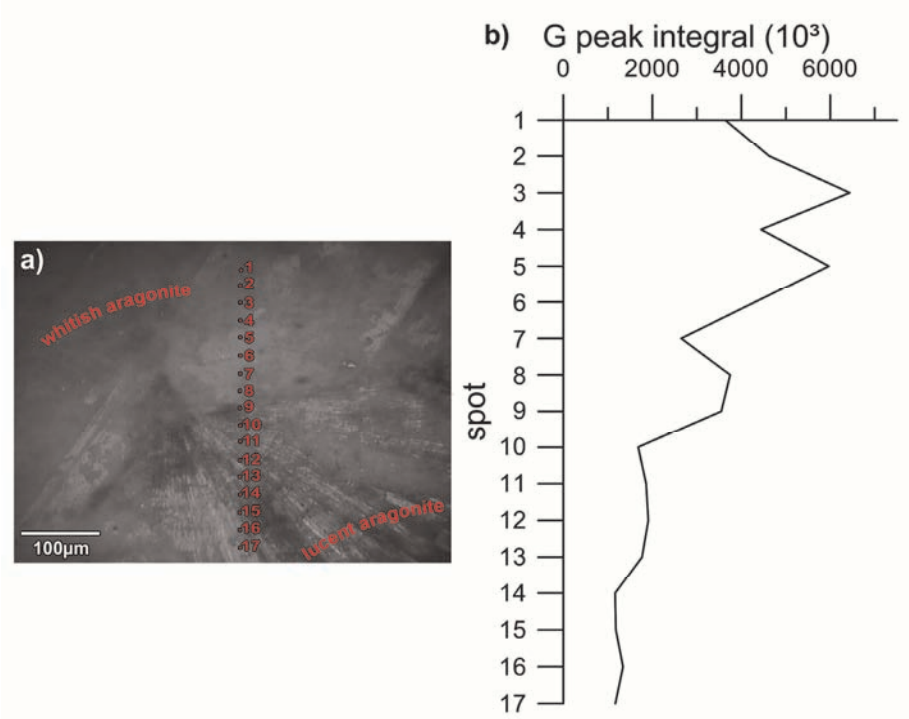

Fig. 7: Raman line profile of Hydrate Ridge microbialite using UV-laser: (**a**) UV-camera image of whitish aragonite and lucent aragonite with marked line profile spots, (**b**) diagram of G peak integral *vs.* spot number (G peak integral = 1548–1640 cm^{-1}).

Conclusions

Under the given analytical conditions UV-Raman spectroscopy does not allow for a detailed characterization of the biomarker content of carbonate microbialites. Except for the broad G peak representing disordered carbonaceous material, no peaks specific for individual functional groups or organic compound classes were detected within the carbonate microbialites studied. The difficulty to further characterize organic matter bound in sedimentary rocks might be regarded as a general drawback of current Raman spectroscopy. Similar problems were reported from the analysis of kerogens (Pasteris & Wopenka 2003). Comparison with published biomarker studies shows a much greater capability of GC-MS to identify distinctive biosignatures of methanotrophic consortia in the microbialite phases. On the other hand, Raman spectroscopy clearly resolved the differences in organic matter content of distinct microbialite phases. Raman spectroscopy can therefore be regarded useful to distinguish fossilized biofilms from precipitates that were not directly mediated by microorganisms. Another advantageous feature of Raman spectroscopy is its capability to simultaneously analyze the mineralogy and organic matter content of the microbialite phases at the microscopic level, and without the need of elaborate sample preparation. The results of this study thus demonstrate that the different techniques cannot replace each other, but should rather be used in conjunction in geobiological studies.

Acknowledgements

We acknowledge with gratitude the anonymous reviewer for constructive comments that helped improve the manuscript. We are grateful to Volker Liebetrau (GEOMAR, Kiel) and Joachim Reitner (University of Göttingen) for providing the Hydrate Ridge samples, Gernot Arp (University of Göttingen) for the Münder Formation samples, and Veit-Enno Hoffmann for the Lincoln Creek Formation samples. We furthermore wish to thank Richard Seifert (University of Hamburg) as chief scientist on cruise POS 317-2 through which the Black Sea microbial mat samples were retrieved. Financial support by the Deutsche Forschungsgemeinschaft through grants BL 971/1-3, TH 713/3-1, and FOR 571 is kindly acknowledged.

References

Arp, G.; Ostertag-Henning, C.; Yücekent, S.; Reitner, J. & Thiel, V. (2008): Methane-related microbial gypsum calcitization in stromatolites of a marine evaporative setting (Münder Formation, Upper Jurassic, Hils Syncline, north Germany). *Sedimentology* **55** (5): 1227-1251. http://dx.doi.org/10.1111/j.1365-3091.2007.00944.x

Barnes, R. O. & Goldberg, E. D. (1976): Methane production and consumption in anoxic marine sediments. *Geology* **4** (5): 297-300. http://dx.doi.org/10.1130/0091-7613(1976)4<297:MPACIA>2.0.CO;2

Birgel, D.; Himmler, T.; Freiwald, A. & Peckmann, J. (2008): A new constraint on the antiquity of anaerobic oxidation of methane: Late Pennsylvanian seep limestones from southern Namibia. *Geology* **36** (7): 543-546. http://dx.doi.org/10.1130/G24690A.1

Blumenberg, M.; Seifert, R.; Reitner, J.; Pape, T. & Michaelis, W. (2004): Membrane lipid patterns typify distinct anaerobic methanotrophic consortia. *Proceedings of the National Academy of Sciences* **101** (30): 11111-11116. http://dx.doi.org/10.1073/pnas.0401188101

Campbell, K. A.; Farmer, J. D. & Des Marais, D. (2002): Ancient hydrocarbon seeps from the Mesozoic convergent margin of California: carbonate geochemistry, fluids and palaeoenvironments. *Geofluids* **2** (2): 63-94. http://dx.doi.org/10.1046/j.1468-8123.2002.00022.x

Egorov, V. N.; Luth, U.; Luth, C. & Gulin, M. B. (1998): Gas seeps in the submarine Dnieper Canyon, Black Sea: acoustic, video and trawl data. In: Luth, U.; Luth, C.; & Thiel, H. (eds.): *Methane Gas Seep Explorations in the Black Sea (MEGASEEBS), Project Report. Berichte aus dem Zentrum für Meeres- und Klimaforschung* **14**: 11-21.

Frech, R.; Wang, E. C. & Bates, J. B. (1980): The i.r. and Raman spectra of $CaCO_3$ (aragonite). *Spectrochimica Acta Part A: Molecular Spectroscopy* **36** (10): 915-919. http://dx.doi.org/10.1016/0584-8539(80)80044-4

Frosch, T.; Tarcea, N.; Schmitt, M.; Thiele, H.; Langenhorst, F. & Popp, J. (2007): UV Raman Imaging - A Promising Tool for Astrobiology: Comparative Raman Studies with Different Excitation Wavelengths on SNC Martian Meteorites. *Analytical Chemistry* **79** (3): 1101-1108. http://dx.doi.org/10.1021/ac0618977

Gal'chenko, V. F. (2004): On the Problem of Anaerobic Methane Oxidation. *Microbiology* **73** (5): 698-707. [translation of *Microbiologyia*]

Greinert, J.; Bohrmann, G. & Elvert, M. (2002): Stromatolitic fabric of authigenic carbonate crusts: result of anaerobic methane oxidation at cold seeps in 4,850 m water depth. *International Journal of Earth Sciences* **91** (4): 698-711. http://dx.doi.org/10.1007/s00531-001-0244-9

Greenwood, P. F.; George, S. C. & Hall, K. (1998): Applications of laser micropyrolysis-gas chromatography-mass-spectrometry. *Organic Geochemistry* **29** (5-7): 1075-1089. http://dx.doi.org/10.1016/S0146-6380(98)0010-6

Greinert, J.; Bohrmann J. G. & Suess, E. (2001): Gas Hydrate-Associated Carbonates and Methane-Venting at Hydrate Ridge: Classification, Distribution, and Origin of Authigenic Lithologies. In: Natural Gas Hydrates: Occurrence, Distribution, and Detection. *Geophysical Monograph Series* **124**: 99-113. http://dx.doi.org/10.1029/GM124p0099

Hagemann, A.; Leefmann, T.; Peckmann, J.; Hoffmann, V.-E. & Thiel, V. (2013): Biomarkers from individual carbonate phases of an Oligocene cold-seep deposit, Washington State, USA. *Lethaia* **46** (1): 7-18. http://dx.doi.org/10.1111/j.1502-3931.2012.00316.x

Iversen, N. & Jörgensen, B. B. (1985): Anaerobic methane oxidation rates at the sulfate-methane transition in marine sediments from Kattegat and Skagerrak (Denmark). *Limnology and Oceanography* **30** (5): 944-955.

Kiefer, W. (1995): Special techniques and applications. In: Schrader, B. (ed.): *Infrared and Raman Spectroscopy - Methods and Applications*. Weinheim (VCH): 465-517.

Kneipp, K.; Kneipp, H.; Itzkan, I.; Dasari, R. R. & Feld, M. S. (1999): Surface-enhanced non-linear Raman scattering at the single-molecule level. *Chemical Physics* **247** (1): 155-162. http://dx.doi.org/10.1016/S0301-0104(99)00165-2

Leefmann, T.; Bauermeister, J.; Kronz, A.; Liebetrau, V.; Reitner, J. & Thiel, V. (2008): Miniaturized biosignature analysis reveals implications for the formation of cold seep carbonates at Hydrate Ridge (off Oregon, USA). *Biogeosciences* **5** (3): 731-738. http://dx.doi.org/10.5149/bg-5-731-2008

Michaelis, W.; Seifert, R.; Nauhaus, K.; Treude, T.; Thiel, V.; Blumenberg, M.; Knittel, K.; Gieseke, A.; Peterknecht, K.; Pape, T.; Boetius, A.; Amann, R.; Jørgensen, B. B.; Widdel, F.; Peckmann, J.; Pimenov, N. V. & Gulin, M. B. (2002): Microbial Reefs in the Black Sea Fueled by Anaerobic Oxidation of Methane. *Science* **297** (5583): 1013-1015. http://dx.doi.org/10.1126/science.1072502

Pasteris, J. D. & Wopenka, B. (2003): Necessary, but Not Sufficient: Raman Identification of Disordered Carbon as a Signature of Ancient Life. *Astrobiology* **3** (4): 727-738. http://dx.doi.org/10.1089/153110703322736051

Pearson, M. J.; Hendry, J. P.; Taylor, C. W. & Russell, M. A. (2005): Fatty acids in sparry calcite fracture fills and microsparite cement of septarian diagenetic concretions. *Geochimica et Cosmochimica Acta* **69** (7): 1773-1786. http://dx.doi.org/10.1016/j.gca.2004.09.024

Peckmann J.; Goedert, J. L.; Thiel, V.; Michaelis, W. & Reitner, J. (2002): A comprehensive approach to the study of methane-seep deposits from the Lincoln Creek Formation, western Washington State, USA. *Sedimentology* **49** (4): 855-873. http://dx.doi.org/10.1046/j.1365-3091.2002.00474.x

Peckmann, J.; Reimer, A.; Luth, U.; Luth, C.; Hansen, B. T.; Heinicke, C.; Hoefs, J. & Reitner, J. (2001): Methane-derived carbonates and authigenic pyrite from the northwestern Black Sea. *Marine Geology* **177** (1-2): 129-150. http://dx.doi.org/10.1016/S0025-3227(91)00128-1

Peckmann, J. & Thiel, V. (2004): Carbon cycling at ancient methane–seeps. *Chemical Geology* **205** (3-4): 443-467. http://dx.doi.org/10.1016/j.chemgeo.2003.12.025

Pimenov, N. V.; Rusanov, I. I.; Poglazova, M. N.; Mityushina, L. L.; Sorokin, D. Y.; Khmelenina, V. N. & Trotsenko, Y. A. (1997): Bacterial mats on coral-like structures at methane seeps in the Black Sea. *Microbiology* **66** (3): 354-360. [translation of *Mikrobiologiya*)]

Polikarpov, G. G.; Egorov, V. N.; Gulin, S. B.; Gulin M. B.; Stokozov N. A. (1992): Gas seeps from the bottom of the Black Sea - A new object of molismology. In: Polikarpov, G. G. (ed.): *Molismology of the Black Sea*. Kiev (Nauka): 10-28.

Reeburgh, W. S. (1976): Methane consumption in Cariaco Trench waters and sediments. *Earth and Planetary Science Letters* **28** (3): 337-344. http://dx.doi.org/10.1016/0012-821X(76)90195-3

Reitner, J.; Peckmann, J.; Reimer, A.; Schumann, G. & Thiel, V. (2005): Methane-derived carbonate build-ups and associated microbial communities at cold seeps on the lower Crimean shelf (Black Sea). *Facies* **51**: 66-79. http://dx.doi.org/10.1007/s10347-005-0059-4

Suess, E.; Carson, B.; Ritger, S. D.; Moore, J. C.; Jones, M. L. & Kulm, L. D. (1985): Biological communities at vent sites along the subduction zone off Oregon. *Biological Society of the Washington Bulletin* **6**: 475-484.

Tarcea, N.; Harz, M.; Rosch, P.; Frosch, T.; Schmitt, M.; Thiele, H.; Hochleitner, R. & Popp, J. (2007): UV Raman spectroscopy – A technique for biological and mineralogical *in situ* planetary studies. *Spectrochimica Acta (A: Molecular and Biomolecular Spectroscopy)* **68** (4): 1029-1035. http://dx.doi.org/10.1016/j.saa.2007.06.051

Teichert, B. M. A.; Bohrmann, G. & Suess, E. (2005): Chemoherms on Hydrate Ridge – Unique microbially-mediated carbonate build-ups growing into the water column. *Palaeogeography, Palaeoclimatology, Palaeoecology* **227** (1-3): 67-85. http://dx.doi.org/10.1016/j.palaeo.2005.04.029

Thiel, V.; Heim, C.; Arp, G.; Hahmann, U.; Sjövall, P. & Lausmaa, J. (2007): Biomarkers at the microscopic range: ToF-SIMS molecular imaging of Archaea-derived lipids in a microbial mat. *Geobiology* **5** (4): 413-421. http://dx.doi.org/10.1111/j.1472-4669.2007.00119.x

Toporski, J. K. W.; Steele, A.; Westall, F.; Avci, R.; Martill, D. M. & McKay, D. S. (2002): Morphologic and spectral investigation of exceptionally well-preserved bacterial biofilms from the Oligocene Enspel formation, Germany. *Geochimica et Cosmochimica Acta* **66** (10): 1773-1791. http://dx.doi.org/10.1016/S0016-7037(01)00870-5

Urmos, J.; Sharma, S. K. & Mackenzie F. T. (1991): Characterization of some biogenic carbonates with Raman spectroscopy. *American Mineralogist* **76** (3-4): 641-646.

Valentine, D. L. & Reeburgh, W. S. (2000): New perspectives on anaerobic methane oxidation. *Environmental Microbiology* **2** (5): 477-484. http://dx.doi.org/10.1046/j.1462-2920.2000.00135.x

Werne, J. P.; Haese, R. R.; Zitter, T.; Aloisi, G.; Bouloubassi, I.; Heijs, S.; Fiala-Médioni, A.; Pancost, R. D.; Sinninghe Damsté, J. S.; De Lange, G.; Forney, L. J; Gottschal, J. C.; Foucher, J.-P.; Mascle, J. & Woodside, J. (2004): Life at cold seeps: a synthesis of biogeochemical and ecological data from Kazan mud volcano, eastern Mediterranean Sea. *Chemical Geology* **205** (3-4): 367-390. http://dx.doi.org/10.1016/j.chemgeo.2003.12.031

Cite this article: Leefmann, T.; Blumenberg, M.; Schmidt, B. C. & Thiel, V. (2014): Raman spectroscopy of biosignatures in methane-related microbialites. *In:* Wiese, F.; Reich, M. & Arp, G. (eds.): "Spongy, slimy, cosy & more…". Commemorative volume in celebration of the 60th birthday of Joachim Reitner. *Göttingen Contributions to Geosciences* **77**: 113–122.

http://dx.doi.org/10.3249/webdoc-3922